PHYSICAL REVIEW B **94**, 064431 (2016)

Variable variance Preisach model for multilayers with perpendicular magnetic anisotropy

A. F. Franco,[1] C. Gonzalez-Fuentes,[1] R. Morales,[2,3] C. A. Ross,[4] R. Dumas,[5] J. Åkerman,[5,6] and C. Garcia[1,*]
[1]*Department of Physics, Technical University Federico Santa María, 2390123 Valparaiso, Chile*
[2]*Department of Chemical Physics & Materials, University of the Basque Country UPV/EHU, 48940 Leioa, Spain*
[3]*IKERBASQUE, Basque Foundation for Science, 48011 Bilbao, Spain*
[4]*Department of Materials Science and Engineering, Massachusetts Institute of Technology, Cambridge, Massachusetts 02139, USA*
[5]*Physics Department, University of Gothenburg, 412 96 Gothenburg, Sweden*
[6]*Materials Physics, School of ICT, Royal Institute of Technology (KTH), 164 40 Kista, Sweden*
(Received 21 January 2016; revised manuscript received 28 June 2016; published 29 August 2016)

We present a variable variance Preisach model that fully accounts for the different magnetization processes of a multilayer structure with perpendicular magnetic anisotropy by adjusting the evolution of the interaction variance as the magnetization changes. We successfully compare in a quantitative manner the results obtained with this model to experimental hysteresis loops of several $[CoFeB/Pd]_n$ multilayers. The effect of the number of repetitions and the thicknesses of the CoFeB and Pd layers on the magnetization reversal of the multilayer structure is studied, and it is found that many of the observed phenomena can be attributed to an increase of the magnetostatic interactions and subsequent decrease of the size of the magnetic domains. Increasing the CoFeB thickness leads to the disappearance of the perpendicular anisotropy, and such a minimum thickness of the Pd layer is necessary to achieve an out-of-plane magnetization.

DOI: 10.1103/PhysRevB.94.064431

I. INTRODUCTION

Throughout the last decade, materials with perpendicular magnetic anisotropy (PMA) have been of great interest to the scientific community due to their applications in magnetic recording media [1–4]. Recently, this interest has shifted to PMA spin valves and magnetic tunnel junctions (MTJs) due to their potential in reducing the switching energy while preserving thermal stability in spin-torque transfer (STT) magnetic random access memory (MRAM) applications [5–10]. These devices could improve current CMOS processor cache technology by lowering power consumption at sub-20-nm nodes [11–13]. Furthermore, PMA thin films are also of great interest for spin-torque oscillators due to the formation of dynamic droplet solitons [14–17] and their capabilities in generating zero field rf signals with increased output power [18–20]. Thus the importance of understanding the underlying physics related to PMA materials is clear, and many experimental and theoretical studies have been done on this topic [21–25].

Through the use of field-dependent magnetization techniques, unique switching mechanisms have been identified for materials with PMA [21], and theoretical efforts have successfully reproduced the observed behavior in a qualitative manner [25,26]. However, quantitative analysis of the field dependence of magnetization in materials with PMA remains a challenge. In theory, micromagnetic simulations can be used to reproduce the hysteresis loops. However, due to the random distributions of defects and surface roughness, a micromagnetic approach is impractical due to the prohibitively long simulation times required. Numerical calculations and semianalytical hysteresis models like the Preisach, Jiles-Atherton, and vector-hysteresis models have been used successfully to characterize qualitatively and quantitatively different kinds of materials and magnetic arrays by modeling experimental hysteresis loops [27–31]. However, none of the models is able to properly describe the magnetization switching of a thin film material with PMA. Phase field type models such as the one described by Ref. [32] have the potential to reduce simulation times and could be used as an intermediate description between micromagnetic simulations and the various existing semianalytical hysteresis models.

In this paper, we propose an implementation of the variable variance Preisach model (VVPM) [33] that fully accounts for the different magnetization processes of a multilayer with PMA, and successfully compare it in a quantitative manner to experimental hysteresis loops of a $[CoFeB/Pd]_n$ multilayer. This model allows us to identify whether a multilayer structure has significant in-plane components of the magnetization, and gives insights into the physics governing the different magnetization reversal mechanisms.

Furthermore, we explain the changes that arise when the thicknesses of the constituent layers are changed, as well as the effect of the number of [CoFeB/Pd] bilayers. Finally, we show that the magnetostatic interactions are extremely important in determining the behavior of the magnetization in multilayer systems with PMA, and discuss how the behavior is related to the domain wall energy, the magnetostatic interactions, and the surface and volume anisotropy.

II. PREISACH MODEL

Preisach-type models use a phenomenological approach to study hysteretic systems. The system is described by an infinite number of fundamental components called hysterons. Each hysteron has a square hysteresis cycle, with an associated coercive field H_C and interaction field H_B, as shown in Fig. 1. These fields describe the system in terms of stored energy versus energy dissipated in Barkhausen jumps [34]. When applied to thin films with PMA, it becomes evident that the bistable hysterons are directly related to the up and down states of

*Corresponding author: carlos.garcia@usm.cl

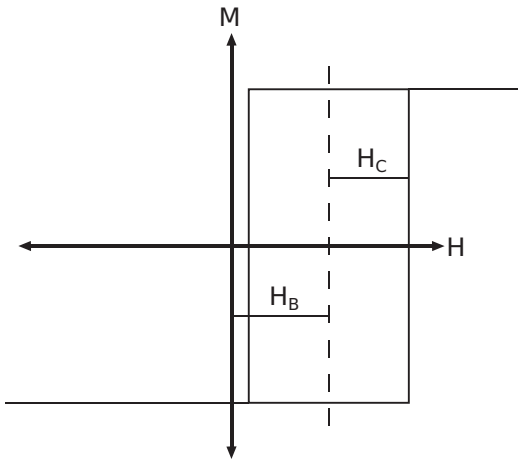

FIG. 1. Square hysteresis cycle of a hysteron, with the associated coercive field H_C and interaction field H_B.

the domains within the material. This allows us to model PMA materials by using a Preisach-type model (as explained below), and to fully account for the different mechanisms governing the magnetization reversal.

The magnetization M for a given applied field is obtained by adding the individual contributions of all the hysterons using the expression

$$\frac{M}{M_s} = \int_0^\infty dH_C \left[\int_{-\infty}^{b(H_c)} p(H_C, H_B) dH_B - \int_{b(H_c)}^{\infty} p(H_C, H_B) dH_B \right], \quad (1)$$

where M_s is the saturation magnetization. The boundary line $b(H_C)$ identifies the state and the history of the system. The major hysteresis loop is given by

$$b(H_C) = H \pm H_C, \quad (2)$$

where the $+$ sign represents the down cycle, the $-$ sign the up cycle, and H is the external applied field. A detailed explanation regarding the selection of $b(H_C)$ which accounts for the history of the system and allows for the calculation of minor hysteresis loops can be found in [34]. The Preisach distribution $p(H_C, H_B)$ represents all the microstructural and magnetic features affecting the magnetization reversal process [34,35]. We assume that H_C and H_B are statistically independent, and thus the Preisach distribution $p(H_C, H_B)$ is written as the product of the distribution of coercive fields $f(H_C)$ and the distribution of interaction fields $g(H_B)$, as given by

$$p(H_C, H_B) = f(H_C) g(H_B). \quad (3)$$

For systems described by the classical Preisach model (CPM), these distributions generally take the form of well known probability distributions, e.g., Gaussian and log-normal distributions [34,36,37]. In thin films with PMA, the distribution of the coercivities can be related to the distribution of defects throughout the sample, and the average coercive field depends on the PMA.

However, it has been shown [33,38,39] that strong interactions affect the shape of $g(H_B)$, leading to a distribution that varies with the magnetization of the film. This prevents the CPM from correctly describing the hysteresis of strongly interacting magnetic systems. As an additional consequence of these interactions, it also has been found [40–42] that the first order reversal curves (FORC) diagrams are equivalent to the Preisach distribution only if the system is correctly described by the CPM.

If one focuses only on major hysteresis loops and ignores higher-order reversal curves (such as those represented by the FORC diagrams), it should be possible to find a Preisach distribution which reproduces these loops. However, in the case of thin film multilayers with PMA, this would lead to Preisach distributions with little to no physical meaning due to the complex relaxation mechanisms associated with these systems (see Sec. IV A).

For thin films with in-plane magnetization or particulate ensembles with random orientations, it has been shown [38,42,43] that the ensemble of interactions follows a multipeaked distribution, which varies with the magnetization state of the sample. To our knowledge, such mapping of the interactions has not been properly studied for thin-film multilayers with PMA. However, previous experiments used to formulate the VVPM [33] suggest that in systems with PMA and large lateral sizes the mean interaction remains zero, and $g(H_B)$ is given by a Gaussian distribution with a variance that evolves with the magnetization following

$$\sigma_B = \sigma_a + \sigma_b |m|^k, \quad (4)$$

where σ_a and σ_b are constants.

Furthermore, it is well known that complex spatiotemporal fluctuations related to the collective dynamics of domain walls during the magnetization switching cannot be ignored in magnetization reversal and hysteresis process. Models based on probability distributions (such as Preisach-type models) are unsuitable to properly describe the magnetization reversal in systems where such fluctuations are present. The most notable of these fluctuations is the Barkhausen effect, where discontinuities in the magnetization reversal arise from irregular fluctuations in the motion of a domain boundary [44]. Nonetheless, if we approach the magnetic relaxation as a sum of individual Barkhausen jumps independent of field rate, the magnetization reversal is dominated by the distribution of pinning fields throughout the sample [45]. It has been shown [34,46,47] that the long-range magnetostatic interactions are the dominant contribution in the distribution of these pinning fields in thin films with PMA. Additionally, these magnetostatically driven pinning fields limit the length of Barkhausen processes [32,46,47]. Thus, assuming that the individual relaxation events take place on a time scale much smaller than the time scale over which the applied field changes significantly, the long-range dipolar interactions are the dominant mechanism for the magnetization reversal of thin films with PMA and the effect of the short-range fluctuations of the domain walls can be ignored, providing justification for the application of Preisach-type hysteresis models.

Reversible magnetization

In general, Preisach-type models only describe changes in the magnetization due to the instantaneous irreversible up-down (or down-up) changes in the magnetization of the

hysterons, therefore the reversible magnetization due to the elastic distortions of the domain structure has to be treated separately. This can be done by approximating the reversible magnetization to a Langevin function [48], where the total magnetization M is given by

$$M = (1 - x)M_{\text{irr}} + x M_{\text{rev}}. \tag{5}$$

M_{irr} is the irreversible magnetization given by [Eq. (1)], M_{rev} is the reversible magnetization given by

$$\frac{M_{\text{rev}}}{M_s} = L\left[\frac{H \mp \bar{H}_C}{a}\right], \tag{6}$$

and x represents the proportion of the reversible magnetization. In Eq. (6), L is the Langevin function. The minus(plus) sign is taken for the down(up) half cycle, and a is a shape parameter dependent on the temperature and the material properties [49].

III. EXPERIMENTAL METHODS

$[Co_{40}Fe_{40}B_{20}(t_{\text{CoFeB}})/Pd(t_{\text{Pd}})]_n$ films were deposited on thermally oxidized Si(100) substrates using confocal DC magnetron sputtering at ambient temperature in a chamber with a base pressure better than 2×10^{-8} Torr and at an Ar working pressure of 5 mTorr. t_{CoFeB} and t_{Pd} represent the thickness of the CoFeB and Pd layers, respectively, and n is the number of repetitions of the [CoFeB/Pd] bilayer system.

The films were grown on a Ta(20 Å)/ Pd(20 Å) seed layer and capped with 5 nm of Pd to protect the surface from oxidization. The thin Ta layer allows for greater mobility of the deposited atoms [50,51] and an improved fcc-(111) orientation of the Pd layer deposited just above, thus improving the PMA of the CoFeB/Pd multilayers. We prepared three series using CoFeB (the target composition was 40-40-20 atomic %) as a soft magnetic material as follows:

(1) $[Co_{40}Fe_{40}B_{20}(3\text{ Å})/Pd(10\text{ Å})]_n$, where $n = 5, 10, 15$;

(2) $[Co_{40}Fe_{40}B_{20}(t_{\text{CoFeB}})/Pd(10\text{ Å})]_5$, where $t_{\text{CoFeB}} = 2, 3, 4, 5$ Å;

(3) $[Co_{40}Fe_{40}B_{20}(3\text{ Å})/Pd(t_{\text{Pd}})]_5$, where $t_{\text{Pd}} = 6, 8, 10, 15, 60$ Å.

Magnetization measurements were performed at room temperature using a PMC MicroMag 2900 alternating gradient magnetometer (AGM) with the magnetic field applied either in plane or out of plane. Magnetic domain structure was imaged using an Evico Magnetics Kerr Microscope with a highly stable and intense Xenon short arc light source, with a maximum optical resolution of about 300 nm. A maximum perpendicular magnetic field of 9200 Oe was provided by an electromagnet.

IV. FORMULATION AND PHYSICAL EXPLANATION OF THE MODEL

A. Relaxation mechanisms

It is known that the relaxation mechanisms of the magnetization of multilayer systems with PMA change with the magnetization of the structure [21,52–54]. In the following, we provide a brief summary of this evolution and a more complete discussion can be found in [21]. First, small domains nucleate in localized sections of the sample due to a stochastic relaxation of the magnetization due to thermal effects [55–57]. These domains serve as nucleation centers for labyrinth domains, inducing a sharp change in the magnetization of the structure. After the system is populated with these domains, the relaxation takes place by growth of the relaxed domains through the motion of the domain walls. Finally, when the growth of the domains is no longer energetically preferred, the relaxation is performed by annihilation of the remaining nonrelaxed labyrinth domains. From this point forward, we refer to the different regimes as the L regime (Labyrinth domain nucleation), W regime (domain Wall motion), and A regime (domain Annihilation). Furthermore, we refer to the transition from the L regime to the W regime and from the W regime to the A regime as the LW and WA transitions, respectively.

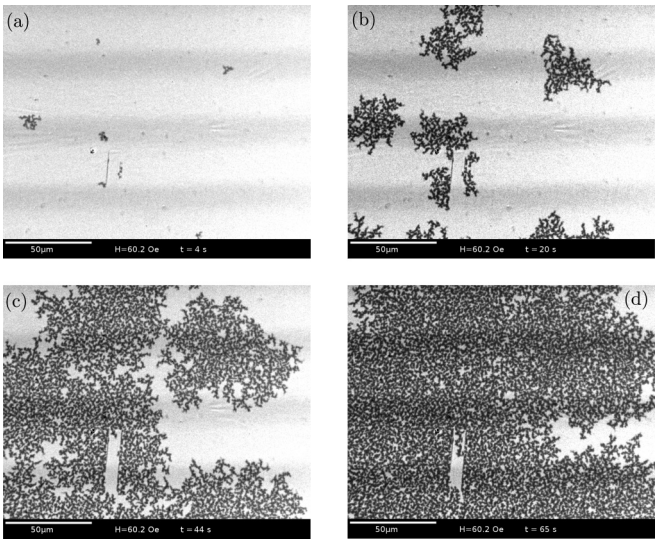

FIG. 2. Kerr microscopy image of the evolution of the labyrinth magnetic domains of a reversing [CoFeB(3 Å)/Pd(10 Å)]$_5$ multilayer system with PMA for (a) $t = 4$, (b) 20, (c) 44, and (d) 65 s after the application of a perpendicular applied field $H = 60.2$ Oe. White (black) indicates negative (positive) saturation.

Figure 2 shows the evolution of the magnetic domains of the [CoFeB(3 Å)/Pd(10 Å)]$_5$ sample for different times after an external field of $H = 60.2$ Oe is applied opposite to the magnetization of the negatively saturated sample. We can clearly see the nucleation of small domains [Fig. 2(a)], which serve as nucleation centers for the labyrinth domains [Fig. 2(b)]. These domains eventually span the entire sample [Figs. 2(c) and 2(d)], confirming the well-known relaxation mechanisms typical of multilayer thin films with PMA. We have found that to obtain a physically meaningful Preisach distribution which describes the hysteresis cycles of the multilayer system $[Co_{40}Fe_{40}B_{20}(t_{\text{CoFeB}})/Pd(t_{\text{Pd}})]_n$, it is necessary to separately account for the different relaxation mechanisms.

We emphasize that a given magnetization state in a thin film with PMA is composed mostly of a combination of up/down states distributed spatially throughout the structure. This means that for these systems, the hysterons composing the Preisach distribution are directly related to the spatial distribution of the up/down magnetization states. Consequently, the distribution of coercivities and interactions composing the Preisach distribution are directly related to the spatial distribution of coercivities and interactions throughout the sample, respectively.

B. Distribution of coercivities

It has been shown that a Gaussian distribution of the anisotropies is a reasonable choice to account for the structural disorder in thin films with PMA [25]. The distribution of coercivities is assumed to take the following form:

$$f(H_C) = (1 - p_d)\frac{1}{\sqrt{2\pi}\sigma_C}\exp\left[-\frac{(H_C - \bar{H}_C)^2}{2\sigma_C^2}\right] + p_d\frac{1}{\sqrt{2\pi}\sigma_D}\exp\left[-\frac{(H_C - \bar{H}_D)^2}{2\sigma_D^2}\right], \quad (7)$$

where σ_C is the variance of the coercivities, and $\bar{H}_C$ is the average coercive field of the system.

Equation (7) has an additional term which represents the defects within the samples. $\bar{H}_D$ is their average coercive field, σ_D is the variance of their coercive fields, and p_d is the proportion of defects. The defect coercivity $\bar{H}_D$ is independent of the average coercive field $\bar{H}_C$ in order to separate the contribution of the defects from that of the PMA.

A possible origin of these defects is the roughness of the Si substrate, which is of the order of 18 Å. When this roughness is comparable to the total thickness of the magnetic material (nominal thickness of the CoFeB times the number of repetitions), local variability in the structure is introduced. When combined with the natural roughness of the interface, these changes lead to local variations of the PMA throughout the sample.

Equation (7) does not depend on the magnetization state, and thus does not account for the evolution of the relaxation mechanisms explained in Sec. IV A. Indeed, the distribution of anisotropies arises from local changes in the physical configuration of the multilayer and should not depend on the magnetic state of the structure.

C. Distribution of interactions

As stated previously, the origin of the nucleation sites which initiate the different reversal regimes is thermally activated stochastic magnetic relaxation [55–57]. Nonetheless, once the nucleation sites are created, the relaxation processes and mechanisms are governed by the interactions throughout the system [25,26,52,54,58,59].

Other works on thin film structures where local relaxation processes arise randomly throughout the sample have shown that the interactions typically follow single or multipeaked distributions [38,39,42,43,60–62]. We assume the simplest case, where the distribution for the interactions is given by the single peak Gaussian distribution:

$$g(H_B) = \frac{1}{\sqrt{2\pi}\sigma_B}\exp\left[-\frac{H_B^2}{2\sigma_B^2}\right], \quad (8)$$

where σ_B is the interaction variance, which depends on the magnetization state of the system [33].

When σ_c is very small, most of the information provided by the Preisach distribution is centered around a very narrow range of H_C. In this case, when solving Eq. (1) for major loops [$b(H_C)$ is given by Eq. (2)], Eq. (8) is indistinguishable from an equivalent distribution $g_p(H_B) = \exp[-(H_B - \bar{H}_B)^2/(2\sigma_{Bp}^2)]/(\sqrt{2\pi}\sigma_{Bp})$, where $\bar{H}_B$ is the mean interaction field, and σ_{Bp} is the variance of the new distribution. For a proper physical description, this mean field should depend linearly on the magnetization state following $\bar{H}_B = \alpha m$, as given by the moving Preisach model (MPM) [35,63,64]. However, we have found that the MPM alone is not able to describe properly the hysteresis cycles of our multilayers with PMA, and a nonlinear dependence of $\bar{H}_B$ with m is necessary. It has been suggested that both the VVPM and MPM are necessary in systems with complex magnetization processes [35], and a two peaked model which can describe their individual and combined contributions (as particular cases) has been formulated previously by Stancu *et al.* [62]. Nonetheless, if both the VVPM and the MPM are used simultaneously to reproduce the major hysteresis loops of our samples, we found that the MPM only adds a fitting parameter α with an effect indistinguishable from the results obtained by the VVPM alone. Hence, we use Eq. (8), where σ_B includes information on both the mean interaction field and the variance of the interactions. Future works could focus on the separation of both contributions by the study of, *e.g.*, FORC diagrams.

Taking into account the existence of the three different relaxation regimes L, W, and A, we have separated the evolution of σ_B in three stages. Each individual stage follows the general expression given by the VVPM [Eq. (4)], and we ensure continuity of σ_B for $-1 < m < 1$. σ_B is then given by

$$\sigma_B^u = \begin{cases} \sigma_a^{\mathrm{L}} + \sigma_b^{\mathrm{L}} m & m < m_{\mathrm{LW}}, \\ \sigma_a^{\mathrm{W}} + \sigma_b^{\mathrm{W}}|m|^{0.1} & m_{\mathrm{LW}} < m < m_{\mathrm{WA}}, \\ \sigma_a^{\mathrm{A}} + \sigma_b^{\mathrm{A}}|m|^{5} & m > m_{\mathrm{WA}} \end{cases} \quad (9)$$

for the up cycle, and

$$\sigma_B^d = \begin{cases} \sigma_a^{\mathrm{L}} - \sigma_b^{\mathrm{L}} m & m > -m_{\mathrm{LW}}, \\ \sigma_a^{\mathrm{W}} - \sigma_b^{\mathrm{W}}|m|^{0.1} & -m_{\mathrm{LW}} > m > -m_{\mathrm{WA}}, \\ \sigma_a^{\mathrm{A}} - \sigma_b^{\mathrm{A}}|m|^{5} & m < -m_{\mathrm{WA}} \end{cases} \quad (10)$$

for the down cycle. σ_a^β and σ_b^β, with $\beta \equiv$ L, W, and A, are given in Eq. (A2). They are functions of the following parameters: the value of σ_B at the zero magnetization state σ_0, the value of σ_B at the start of each half loop σ_{st}, the value of σ_B at the end of each half loop σ_{nd}, the value of m for which the LW transition occurs m_{LW}, and the value of m for which the WA transition occurs m_{WA}.

A phenomenological approach was used to identify each value of the exponent k, similar to recent works treating the modeling of the hysteresis of magnetic materials [28,31,65,66]. More precisely, they were obtained by fitting the measured [CoFeB(3 Å)/Pd(10 Å)]$_{15}$ multilayer, and application of the model to the remaining samples revealed that they remain unchanged as long as there is a negligible in-plane component of the magnetization.

Both m_{LW} and m_{WA} are defined for the up-loop, and the formulation of Eqs. (9) and (10) account for the proper sign and value of m. In practice, the magnetization at which the reversal mechanism changes is not well defined, and there will always be a transitional regime where several mechanisms are present at the same time. Thus the magnetizations m_{LW} and m_{WA} are approximate values. In the following sections, this will be evident in the high estimated errors of the fitted values.

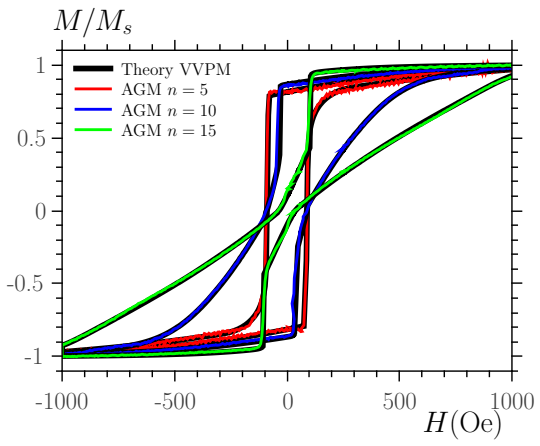

FIG. 3. Hysteresis cycles of a [CoFeB(3 Å)/Pd(10 Å)]$_n$ multilayer system, with $n = 5$, 10, and 15. Comparison of alternating gradient magnetometer measurements with the results from the variable variance Preisach model.

The variations of the local interactions throughout a system with PMA are mostly related to the up-down transitions and the density of domain walls [26,58,60], and thus only irreversible processes are relevant. Furthermore, an increase of temperature results in a reduction of the coercive field [6,67], and thus role of the temperature is taken into account in Eq. (7) through the value of $\bar{H}_C$. Hence only the irreversible magnetization $M_{\rm irr}$ [Eq. (5)] is used to calculate the evolution of σ_B, and consequently, to determine the values of $m_{\rm LW}$ and $m_{\rm WA}$.

V. RESULTS AND DISCUSSION

Figure 3 shows a comparison of the theoretical results obtained with the VVPM given by Eqs. (9) and (10) with the experimental hysteresis cycles for the [CoFeB(3 Å)/Pd(10 Å)]$_n$ samples, with $n = 5$, 10, and 15. An excellent agreement between the two is observed for the three samples, and similar results were obtained for different Pd and CoFeB thicknesses (Figs. 7 and 8). However, when the samples show a strong in-plane magnetization component our model is no longer able to reproduce the experiments. This is because the reversal processes change, and therefore the model has to be changed accordingly to account for the new relaxation mechanisms. Examples of samples with strong in-plane component of the magnetization can be seen in Figs. 7 ($t_{\rm CoFeB} = 5$ Å) and 8 ($t_{\rm Pd} = 6$ Å).

The simulation parameters are summarized in Tables I–III. Of the different simulation parameters, the average coercive field $\bar{H}_C$, the variances σ_C, σ_0, $\sigma_{\rm st}$, and $\sigma_{\rm nd}$, and the magnetizations $m_{\rm LW}$ and $m_{\rm WA}$ are the most relevant when describing the magnetization reversal of a thin film with PMA. In general, we found that besides the defects (which present a high coercive field), the films are of very high quality with a very low distribution of coercivities, and thus σ_C is not listed ($\sigma_C = 1$ Oe for all the samples, which is the lowest resolution that our numerical implementation of the VVPM has for the coercive field). The final value labeled Sat. Corr. is a percentage correction of the saturation magnetization applied to eliminate the mismatch between the measured and theoretical saturation, which may stem from temperature effects. The reversible magnetization [Eq. (6)] was fitted to the sections at the beginning of each half loop before the sharp irreversible switching is observed (Figs. 3, 7, and 8). We obtain a reasonably good agreement with the experiments, and the associated fitting parameters remain mostly on the ranges of $x = 0.2$–0.3 and $a = 200$–300 Oe. However, the reversible magnetization relaxation due to temperature effects is not the focus of this work, and thus the values of these fitting parameters are not specified for each individual sample.

We have estimated the errors linked to each fitting parameter in order to provide a better understanding of the precision of the obtained results. To estimate these errors, individual parameters were varied until it was evident that the calculated hysteresis loops no longer described the experimental measurements. $\bar{H}_C$, σ_0, $\sigma_{\rm st}$, and $\sigma_{\rm nd}$ show very small estimated errors (Tables I–III) of up to 10 Oe, which arise from the small variations in the experimental data due to thermal effects and the experimental setup. From a percentage point of view, some of these errors appear significant. However, due to constraints in the simulation time, our implementation of the VVPM has a maximum precision of 1 Oe for all the variances. Furthermore, due to the small coercivity of our samples, most of the magnetization dynamics happen at low fields, and thus errors of the order of 10 Oe become more relevant. It can be seen that even when the values of the coercivity and the variances increase, the estimated errors stay within the same order of magnitude ($\approx$10 Oe). On the other hand, all the values of $m_{\rm LW}$ and $m_{\rm WA}$ have high estimated errors, which is an indication that the change between the different reversal mechanisms occurs gradually, leading to regimes where more than one mechanism is present.

The defects of almost all the samples had similar average coercive field ($\bar{H}_D = 800$ Oe with varying estimated errors. For the [CoFeB(3 Å)/Pd(15 Å)]$_5$ sample, a slightly different value of $\bar{H}_D = 750 \pm 10$ Oe was used instead), and only the variance σ_D changed from sample to sample. The effect of these defects on the hysteresis cycle is evident in Fig. 4(a) through the gap in the magnetization for high fields ($|H| > 300$ Oe).

In the following, we present an analysis of the measured hysteresis cycles and a comparison with our model, which has

TABLE I. Effect of the number of repetitions on the parameters of the variable variance Preisach model for different [CoFeB(3 Å)/Pd(10 Å)]$_n$ samples.

Sample	$\bar{H}_C$(Oe)	σ_0(Oe)	$\sigma_{\rm st}$(Oe)	$\sigma_{\rm nd}$(Oe)	$m_{\rm LW}$	$m_{\rm WA}$	σ_D(Oe)	Sat. Corr. (%)
[CoFeB(3 Å)/Pd(10 Å)]$_5$	89 ± 1	4 ± 1	3 ± 1	80 ± 10	-0.25 ± 0.75	-0.1 ± 0.6	300 ± 50	5 ± 0.5
[CoFeB(3 Å)/Pd(10 Å)]$_{10}$	85 ± 5	150 ± 10	20 ± 5	250 ± 5	-0.3 ± 0.29	0.55 ± 0.25	200 ± 50	3 ± 0.5
[CoFeB(3 Å)/Pd(10 Å)]$_{15}$	25 ± 5	390 ± 10	50 ± 5	420 ± 10	-0.5 ± 0.1	0.3 ± 0.29	100 ± 50	1 ± 0.3

TABLE II. Effect of the CoFeB thickness on the parameters of the variable variance Preisach model for different [CoFeB(t_{CoFeB})/Pd(10 Å)]$_5$ samples.

Sample	$\bar{H}_C$(Oe)	σ_0(Oe)	σ_{st}(Oe)	σ_{nd}(Oe)	m_{LW}	m_{WA}	σ_D(Oe)	Sat. Corr. (%)
[CoFeB(2 Å)/Pd(10 Å)]$_5$	82 ± 2	10 ± 2	10 ± 2	10 ± 2	–	–	110 ± 10	9 ± 1
[CoFeB(3 Å)/Pd(10 Å)]$_5$	89 ± 1	4 ± 1	3 ± 1	80 ± 10	-0.25 ± 0.75	-0.1 ± 0.6	300 ± 50	5 ± 0.5
[CoFeB(4 Å)/Pd(10 Å)]$_5$	12 ± 3	86 ± 2	15 ± 2	60 ± 10	-0.5 ± 0.1	-0.1 ± 0.09	200 ± 50	3.5 ± 0.5

allowed us to identify different behaviors of the magnetization reversal and the magnetostatic interactions related to changes in the number of repetitions, thickness of the CoFeB, and thickness of the Pd.

A. General discussion

By analyzing the values of the fitting parameters presented in Tables I–III, we can explain the different physical aspects related to the size of the domains, the domain wall density, the magnetostatic interactions, and the number of repetitions in multilayers with PMA. It has been shown theoretically and experimentally [26,52,58] that there is a reduction of the domain size (or thickness in the case of stripe domains) when the number of repetitions of a PMA multilayer increases. This reduction in size has been related to an increase of the interlayer magnetostatic interactions [26,58], and originates from the competition between the latter and the domain wall energy of the system [26,59]. More precisely, the domain wall energy of the system per unit volume decreases with increasing domain size, while the magnetostatic energy per unit volume decreases with decreasing domain size. The energy is thus minimized for the domain size and density of domain walls related to the dominant mechanism, namely, domain wall energy for low n (weak magnetostatic interactions, big domains) and magnetostatic interactions for high n (strong magnetostatic interactions, small domains). Knowing that σ_B (and consequently σ_0, σ_{st}, and σ_{nd}) contains information on both the strength and variance of the interactions, we can relate wide and narrow labyrinth domains to low and high values of σ_B, respectively [e.g., comparing σ_0, σ_{st}, and σ_{nd} for $n = 10$ and 15 in Table I, it is evident that the sample with $n = 10$ has wider labyrinth domains than the sample with $n = 15$ due to the difference of their magnetostatic interaction].

Now we will make use of Fig. 5, which shows a simplified one dimensional magnetization state of the upwards cycle after each stage of the magnetization reversal, namely, (i) saturation [Fig. 5(a)], (ii) L regime [Figs. 2 and 5(b)], (iii) W regime [Fig. 5(c)], and (iv) A regime [Fig. 5(d)]. Figure 5(e) shows the evolution of σ_B^u with the normalized magnetization m for the [CoFeB(3 Å)/Pd(10 Å)]$_n$ samples.

In the saturated state i, the interaction is homogeneous throughout the sample, and thus $\sigma_B^u(m = -1) = \sigma_{st}$ is zero (or very low in real samples), as seen in Fig. 5(e). It increases with the number of layers to represent stronger magnetostatic interactions.

After the nucleation field is reached the system arrives at stage ii, and the magnetization decreases rapidly due to the formation of labyrinth stripe domains in an avalanche process [21]. The disorder of the local magnetization states and the density of the domain walls throughout the sample has increased greatly, leading to different values of the interactions across the sample. This increases σ_B^u following a linear behavior given by the first line of Eqs. (9) and (10) until the magnetization reaches the critical value $m = m_{LW}$. This linear behavior can be observed in Fig. 5(e) for $-1 < m < m_{LW}$.

Further increasing the field will induce motion of the domain walls, as indicated by the small arrows in Fig. 5(c) (stage iii). In a real sample, the shape of the labyrinth domains and thus the density of domain walls remains mostly constant. Hence the interactions observe very low variation. This is represented by the small value of the exponent $k = 0.1$ in the second line of Eqs. (9) and (10). Thus σ_B^u is mostly constant for $m < 0$ and $m > 0$, but a jump in its value is introduced at $m \approx 0$. This behavior can be observed in Fig. 5(e) for $m_{LW} < m < m_{WA}$. In the following discussion we explain the origin of this jump.

It is well known that due to the magnetostatic interaction, magnetic domains become more stable as their size decreases. When $m < 0$, the down domains are bigger than the up domains, while for $m > 0$, the up domains are dominant. That means that due to their size, the up domains are more stable for $m < 0$, and is easier to switch into them from the less stable down domains, hence there is a lower σ_B^u. For $m > 0$, the down domains are more stable, and thus σ_B^u increases because it is now more difficult to induce switching. $m \approx 0$ is a transitional state where both the up and down domains are roughly equally stable, leading to the jump in σ_B^u. In general, $m_{LW} < 0$. Nonetheless, there can be multilayer structures where $m_{LW} > 0$. In such cases, σ_B^u does not demostrate the transitional regime (jump), and it becomes nearly constant with value $2\sigma_0 - \sigma_{st}$.

Another consequence of the increased stability of small domains is a slow variation of the magnetization with the applied field when the domains decrease in size. Thus, once in the A regime (stage iv), the variance changes slowly from $2\sigma_0 - \sigma_{st}$ (for $m = m_{WA}$) to σ_{nd} (for saturation) to represent

TABLE III. Effect of the Pd thickness on the parameters of the variable variance Preisach model for different [CoFeB(3 Å)/Pd(t_{Pd})]$_5$ samples.

Sample	$\bar{H}_C$(Oe)	σ_0(Oe)	σ_{st}(Oe)	σ_{nd}(Oe)	m_{LW}	m_{WA}	σ_D(Oe)	Sat. Corr. (%)
[CoFeB(3 Å)/Pd(10 Å)]$_5$	89 ± 1	4 ± 1	3 ± 1	80 ± 10	-0.25 ± 0.75	-0.1 ± 0.6	300 ± 50	5 ± 0.5
[CoFeB(3 Å)/Pd(15 Å)]$_5$	37 ± 2	75 ± 5	12 ± 1	85 ± 5	0.01 ± 0.05	0.45 ± 0.15	90 ± 70	4.5 ± 0.5
[CoFeB(3 Å)/Pd(60 Å)]$_5$	42 ± 3	12 ± 1	9 ± 1	1 ± 1	-0.21 ± 0.78	-0.19 ± 0.78	200 ± 50	4 ± 0.5

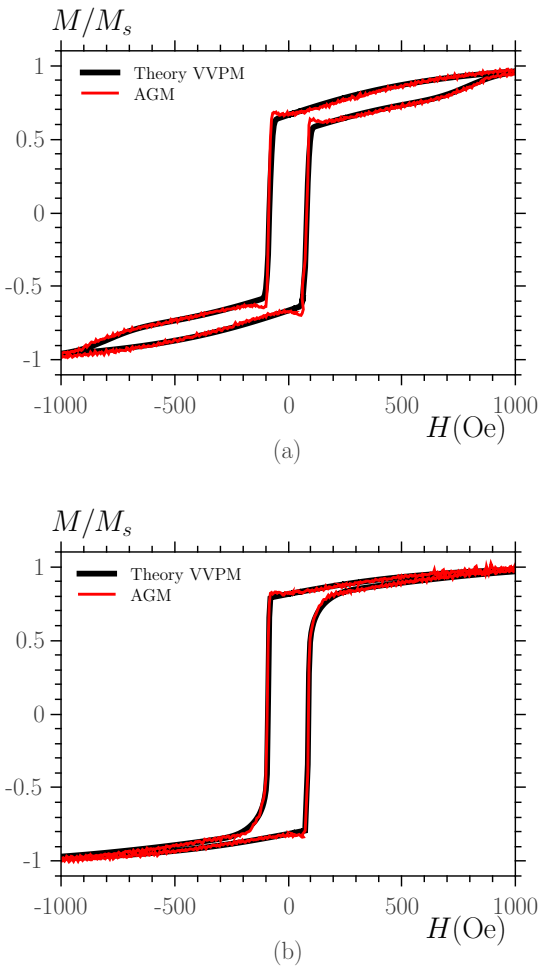

FIG. 4. Measured and calculated hysteresis cycle of [CoFeB(2 Å)/Pd(10 Å)]$_5$ and [CoFeB(3 Å)/Pd(10 Å)]$_5$ multilayer system.

the increased stability of the domains. This slow change in σ_B^u is obtained through the large exponent $k = 5$, as seen in Fig. 5(e) for $m > m_{\mathrm{WA}}$.

As the domains are annihilated the density of domain walls decreases, reducing σ_B^u. From the values in Tables I–III, it can be shown that almost all the samples exhibit a reduction of the variance in the A regime ($\sigma_{\mathrm{nd}} < 2\sigma_0 - \sigma_{\mathrm{st}}$). Only two samples show deviations from this behavior: [CoFeB(2 Å)/Pd(10 Å)]$_5$ and [CoFeB(3 Å)/Pd(10 Å)]$_5$. The [CoFeB(2 Å)/Pd(10 Å)]$_5$ sample exhibits very small magnetostatic interactions due to a small thickness of the magnetic material and a small number of repetitions, and thus the switching regimes are not well defined as the magnetization changes (hence the values of m_{LW} and m_{WA} in Table II are not defined for this sample). This is further confirmed by the square hysteresis loop, as shown in Fig. 4(a).

The hysteresis loop of the [CoFeB(3 Å)/Pd(10 Å)]$_5$ sample is shown in Fig. 4(b). While the squareness of the loop approaches unity, there is a noticeable slope indicating true saturation requires significantly more field. We only were able to reproduce this slope by increasing σ_B in the A regime. A similar behavior in other thin films with PMA has been attributed to pinning of the domains to defects [54] or to the physical domain boundaries in patterned thin films [57], which slows down the magnetization reversal effectively increasing σ_B. This pinning is present as long as there is a sufficiently strong interaction within the sample. Nonetheless, for samples with strong interlayer magnetostatic interactions, the domains become smaller. With smaller domains, the pinning of the magnetization around the defects becomes less relevant, and σ_B decreases instead due to the increased order induced by the domain annihilation.

Finally, one should expect σ_B to be equal for $m = \pm 1$. As seen in Fig. 5(e) this is not the case. This difference comes from the fact that σ_B contains information on both the strength and variance of the interactions. As stated before, as the system reaches saturation and the domains decrease in size they become more stable, which changes the interaction strength seen by an opposite applied field.

B. Number of repetitions

We studied the effect of the number of repetitions n on the hysteresis cycles of [CoFeB(3 Å)/Pd(10 Å)]$_n$ samples, with $n = 5$, 10, 15, and the results are summarized in Table I. The most notable effect is the systematic increase of the variances σ_0, σ_{st}, and σ_{nd}, indicating an increase of the magnetostatic interactions. In fact, as we noted in the previous section, we can attribute several of the different phenomena observed in our samples to the increase of magnetostatic interactions, making it one of the most fundamental contributions that govern the behavior of the magnetization switching in multilayer structures with PMA.

Initially, increasing the number of bilayers does not affect the coercive field. However, once a certain threshold is overcome, the coercivity starts to decrease, in agreement with Jung *et al.* [22] who found a constant $\bar{H}_C$ for a range of small to mid n, and then a reduced $\bar{H}_C$ for large n. To explain

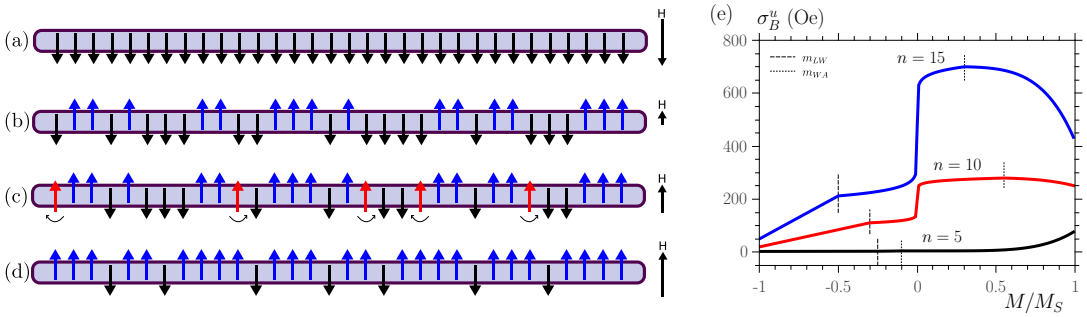

FIG. 5. Stages of the magnetization reversal of a thin film with perpendicular magnetic anisotropy, namely (a) saturation, (b) L regime, (c) W regime, and (d) A regime. (e) Evolution of σ_B for the up cycle of a [CoFeB(3 Å)/Pd(10 Å)]$_n$ multilayer system, with $n = 5$, 10, and 15.

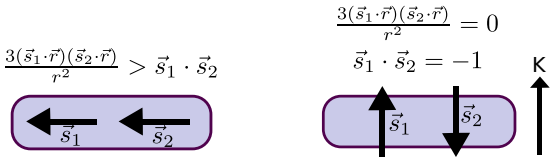

FIG. 6. In plane shape anisotropy (left) and antiferromagnetic interaction (right) contributions of the dipolar interaction to the magnetic ordering of two magnetic moments.

this effect, let us assume a perfect square hysteresis cycle with a coercive field given by the perpendicular anisotropy field given by (in Oe) $H_A \equiv 2K_\perp/M_s$, where $K_\perp$ is the perpendicular anisotropy constant (in erg/cc), and M_s is the saturation magnetization of the magnetic material (in emu/cc). Increasing n affects mostly the volume, and thus H_A (and consequently H_c) remains constant. Nonetheless, as the magnetostatic interactions between the layers increase with n, self-interaction effects start to be relevant, inducing an in-plane shape anisotropy and reducing the coercivity for high n. Increasing n also adds more interfaces to the structure, which should induce variations in the anisotropy constant $K_\perp$. Our model accounts implicitly for these variations through the Preisach distribution and the evolution of the coercivities and interactions with increasing n, thus precise descriptions of the interface anisotropy throughout the sample are not necessary.

Increasing n also decreases the nucleation field, eventually causing magnetization switching even with an opposing applied field (see the negative nucleation field in Fig. 3). This effect has been observed before experimentally and theoretically [21,22,25,53,68]. Knowing that the mechanism of reversal nucleation is identical for all the samples, namely the avalanche of labyrinth domain formation, the presence of a demagnetizing energy can be inferred. Furthermore, it has been shown [25] that this behavior is observed in systems that present only exchange and dipolar interactions. Therefore, by a process of elimination (due to the absence of any material that could produce an antiferromagnetic exchange), we attribute this behavior to the competition between the dipolar interaction and the PMA, which tends to induce an antiparallel state of neaby magnetic moments within a layer, favoring the early formation of nucleation centers and labyrinth domains.

To better understand the origin of this competition, we consider the energy of the dipolar interaction between two magnetic moments $\vec{s}_1$ and $\vec{s}_2$ with equal saturation M_s and connected by the vector $\vec{r}$, given by

$$E_D = -\frac{\mu_0}{4\pi}\frac{M_s^2}{r^3}\left[\frac{3(\vec{s}_1\cdot\vec{r})(\vec{s}_2\cdot\vec{r})}{r^2} - \vec{s}_1\cdot\vec{s}_2\right]. \qquad (11)$$

From the first term within the square brackets in Eq. (11), it is evident that the dipolar energy will be minimized when the magnetic moments are parallel to the vector $\vec{r}$, and thus parallel to each other, as shown in Fig. 6 (left). This leads to the well-known shape anisotropy. However, due to external factors, the magnetic moments could prefer a direction that is not parallel to the connecting vector, and the dipolar interaction tends to align the two magnetic moments in an antiparallel state, as shown in Fig. 6 (right). This antiparallel state has been observed theoretically for thin films [69], spheres [70], and multilayers [71], and experimentally in arrays of elliptical nanomagnets [72]. In our samples, the external factor inducing the antiparallel state is the PMA.

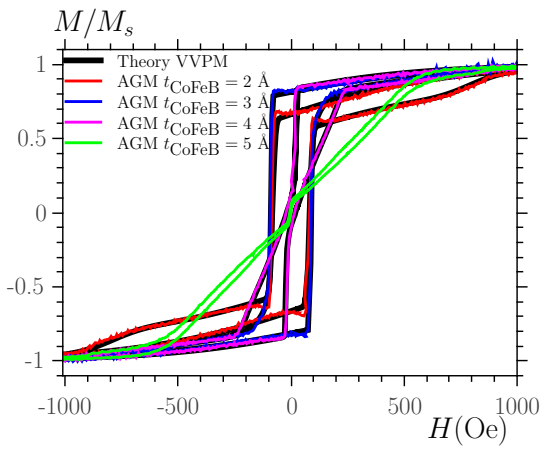

FIG. 7. Hysteresis cycles for a [CoFeB(t_{CoFeB})/Pd(10 Å)]$_5$ multilayer system, with $t_{CoFeB} = 2, 3, 4$, and 5 Å. Comparison of alternating gradient magnetometer measurements with the results from the variable variance Preisach model.

C. CoFeB thickness

The effect of the CoFeB thickness was studied by analyzing different [CoFeB(t_{CoFeB})/Pd(10 Å)]$_5$ samples, with $t_{CoFeB} =$ 2, 3, and 4 Å. The results are summarized in Table II and Fig. 7. The sample with $t_{CoFeB} = 5$ Å shows a strong in-plane component of the magnetization, and thus we were not able to reproduce its hysteresis loop using our model.

Similar to the number of repetitions, increasing the thickness of the CoFeB layer increases the magnetostatic interactions. This increase is more evident in the values of σ_0 and σ_{st} when changing from $t_{CoFeB} = 3$ Å to 4 Å. Nonetheless, when increasing the thickness from 2 Å to 3 Å the increase in the magnetostatic interactions is inferred from the increase in σ_{nd}, which represents stronger pinning to the defects.

Furthermore, a diminution of the coercive field can be observed. This is evidence [73] that the anisotropy of a single Pd/CoFeB/Pd multilayer is given by the combination of an in-plane volumetric component K_v, and an out-of-plane component K_s, which arises from a surface or interface anisotropy present at each CoFeB/Pd interface due to atomic mixing [54,74,75]. This competition eventually leads to the disappearance of the PMA for thicker CoFeB layers, as shown in Fig. 7, where experimental hysteresis cycles for different t_{CoFeB} values are shown. PMA can be observed for $t_{CoFeB} = 2$,3, and 4 Å, with the coercivity being lower in the latter. Furthermore, the hysteresis cycle of the sample with $t_{CoFeB} = 5$ Å clearly shows a shape typical of in-plane magnetization, and thus the PMA has either disappeared or is weak compared to the in-plane volumetric component.

D. Pd thickness

We analyzed different [CoFeB(3 Å)/Pd(t_{Pd})]$_5$ samples to study the effect of the Pd thickness, and the results are summarized in Table III and Fig. 8.

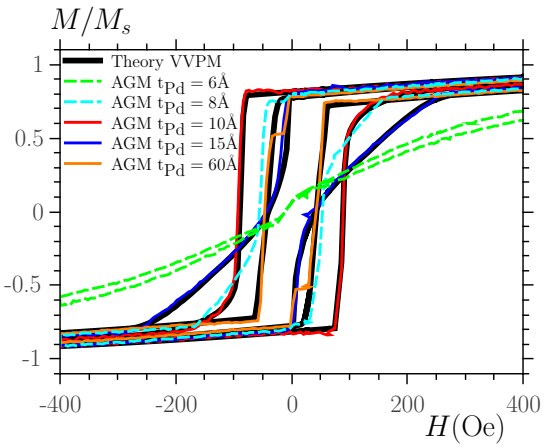

FIG. 8. Hysteresis loops for a [CoFeB(3 Å)/Pd(t_{Pd})]$_5$ multilayer system, with $t_{Pd} = 6$, 8, 10, 15, and 60 Å. Comparison of alternating gradient magnetometer measurements with the results from the variable variance Preisach model.

We observed that a critical value for the thickness of the Pd is necessary to achieve PMA in the sample, as shown in Fig. 8. It can be seen that for $t_{Pd} = 6$ Å the system has an in-plane easy axis, while thicknesses of 10, 15, and 60 Å present a clear indication of PMA and were well described by our model. This critical Pd thickness has been observed by other groups as well [74], and is attributed to smoother CoFeB/Pd interfaces for thicker Pd layers [76]. Moreover, our model does not describe properly the hysteresis loop of the sample with $t_{Pd} = 8$ Å, suggesting a transitional state between in-plane anisotropy and PMA.

Furthermore, a very high Pd thickness leads to a hysteresis loop which is qualitatively very similar to that of a multilayer with low number of repetitions. The increased distance between the magnetic layers reduces the interlayer magnetostatic interactions, and the magnetic behavior of the sample tends towards that of a single Pd/CoFeB/Pd structure, as shown in Fig. 8 for $t_{Pd} = 60$ Å. The initial switching observed in this sample is due to small differences in one of the repetitions, which has a lower coercive field than the rest of the sample, further confirming that each repetition acts individually.

VI. CONCLUSIONS

We have presented a new formulation of the variable variance Preisach model that is able to describe quantitatively the hysteresis cycles of multilayer thin films with PMA, bringing an important improvement over other models which only provide qualitative descriptions. Furthermore, we associate our model with the different magnetization reversal processes observed in the multilayer by adjusting the interaction variance as the magnetization changes. The model provides insight on details of the physics of the magnetization reversal mechanisms and how they are influenced by the interactions. Additionally, our model has the potential to predict the hysteresis loops of multilayer structures with PMA when individual physical parameters such as the thicknesses of the layers, the number of repetitions, and roughness of the interfaces are changed.

We applied our model to [CoFeB/Pd]$_n$ multilayer structures, and we found that in general the variance of the interaction is either constant or follows a simple dependence on the magnetization, but its behavior is greatly dependent upon the reduction of the domain size due to the increase of the magnetostatic interactions, and the enhanced stability of the domains as their size is reduced.

For a small to intermediate number of repetitions, the coercive field is not affected. However, a high number of repetitions eventually induce an in-plane easy axis and reduce the coercivity. An increase of the magnetostatic interactions was also observed. This eventually led to a negative nucleation field, which arises from the competition between the magnetostatic interactions and the PMA.

Furthermore, increasing the thickness of the CoFeB layer also increases the magnetostatic interactions of the structure. Additionally, the coercive field is reduced due to a competition between in-plane volumetric anisotropy and out-of-plane surface anisotropy.

Finally, a minimum thickness of the Pd is necessary to achieve perpendicular magnetization due to the necessity for smooth CoFeB/Pd interfaces. However, a thick Pd layer will decrease the interlayer interaction to the point where each repetition behaves individually.

ACKNOWLEDGMENTS

This work was partially funded by the FONDECYT Postdoctoral Project No. 3150180. C. G. acknowledges the financial support received by FONDECYT Grant No. 1140552 and No. 1130950 and Proyecto Basal FB 0821. Support from the Swedish Research Council (VR), Swedish Foundation for Strategic Research (SSF), the Knut and Alice Wallenberg Foundation, and C-SPIN, a STARnet Center of DARPA and MARCO, is gratefully acknowledged.

APPENDIX: DEFINITION OF THE VVPM VARIANCES

Defining the variances σ_1 and σ_2 as

$$\sigma_1 \equiv \sigma_0 - \sigma_{st}, \quad \sigma_2 \equiv -2\sigma_0 + \sigma_{st} + \sigma_{nd}, \tag{A1}$$

the variances specified in Eqs. (9) and (10) are given by

$$\begin{aligned}
\sigma_a^{L} &= \sigma_0, \quad \sigma_b^{L} = \sigma_1, \\
\sigma_a^{W} &= \sigma_0 + \sigma_1 m_{LW} - \sigma_1 s(m_{LW})|m_{LW}|^{0.1} \Delta_u m_{LW}^{WA}, \\
\sigma_b^{W} &= \sigma_1 s(m) \Delta m_{LW}^{WA}, \\
\sigma_a^{A} &= \sigma_0 + \sigma_1 - \sigma_2 s(m_{WA})|m_{WA}|^{5} \Delta_u m_{WA}^{1}, \\
\sigma_b^{A} &= \sigma_2 s(m) \Delta m_{WA}^{1},
\end{aligned} \tag{A2}$$

with

$$\begin{aligned}
\Delta m_{LW}^{WA} &\equiv \frac{(1 - m_{LW})}{s(m_{WA})|m_{WA}|^{0.1} - s(m_{LW})|m_{LW}|^{0.1}}, \\
\Delta m_{WA}^{1} &\equiv \frac{1}{1.0 - s(m_{WA})|m_{WA}|^{5}}.
\end{aligned} \tag{A3}$$

$s(x)$ is -1 for $x < 0$, 1 for $x > 0$, and 0 for $x = 0$. Equations (A2) and (A3) arise algebraically from ensuring σ_B is continuous from $-1 < m < 1$.

[1] S. N. Piramanayagam, J. Appl. Phys. **102**, 011301 (2007).
[2] O. Hellwig, A. Berger, T. Thomson, E. Dobisz, Z. Z. Bandic, H. Yang, D. S. Kercher, and E. E. Fullerton, Appl. Phys. Lett. **90**, 162516 (2007).
[3] J. M. Shaw, W. H. Rippard, S. E. Russek, T. Reith, and C. M. Falco, J. Appl. Phys. **101**, 023909 (2007).
[4] N. J. Speetzen and B. J. H. Stadler, J. Appl. Phys. **97**, 10N118 (2005).
[5] S. Mangin, D. Ravelosona, J. A. Katine, M. J. Carey, B. D. Terris, and E. E. Fullerton, Nat. Mater. **5**, 210 (2006).
[6] M. Nakayama, T. Kai, N. Shimomura, M. Amano, E. Kitagawa, T. Nagase, M. Yoshikawa, T. Kishi, S. Ikegawa, and H. Yoda, J. Appl. Phys. **103**, 07A710 (2008).
[7] S. Ikeda, K. Miura, H. Yamamoto, K. Mizunuma, H. D. Gan, M. Endo, S. Kanai, J. Hayakawa, F. Matsukura, and H. Ohno, Nat. Mater. **9**, 721 (2010).
[8] D. C. Worledge, G. Hu, D. W. Abraham, J. Z. Sun, P. L. Trouilloud, J. Nowak, S. Brown, M. C. Gaidis, E. J. O'Sullivan, and R. P. Robertazzi, Appl. Phys. Lett. **98**, 022501 (2011).
[9] M. Gajek *et al.*, Appl. Phys. Lett. **100**, 132408 (2012).
[10] H. Yoda, S. Fujita, N. Shimomura, E. Kitagawa, K. Abe, K. Nomura, H. Noguchi, and J. Ito, in *Proceedings of the IEEE International Electron Device Meeting 2012* (IEEE, Piscataway, NJ, 2012), pp. 11.3.1–11.3.4.
[11] S. Kang and K. Lee, Acta Mater. **61**, 952 (2013).
[12] K. Ikegami *et al.*, in *Proceedings of the IEEE International Electron Devices Meeting 2014* (IEEE, Piscataway, NJ, 2014), pp. 28.1.1–28.1.4.
[13] M. Gottwald, J. J. Kan, K. Lee, X. Zhu, C. Park, and S. H. Kang, Appl. Phys. Lett. **106**, 032413 (2015).
[14] M. A. Hoefer, T. J. Silva, and M. W. Keller, Phys. Rev. B **82**, 054432 (2010).
[15] S. M. Mohseni *et al.*, Science **339**, 1295 (2013).
[16] R. H. Liu, W. L. Lim, and S. Urazhdin, Phys. Rev. Lett. **114**, 137201 (2015).
[17] M. Carpentieri, R. Tomasello, R. Zivieri, and G. Finocchio, Sci. Rep. **5**, 16184 (2015).
[18] K. J. Lee, O. Redon, and B. Dieny, Appl. Phys. Lett. **86**, 022505 (2005).
[19] D. Houssameddine, U. Ebels, B. Dela et, M. Brunet, C. Thirion, J.-P. Michel, L. Prejbeanu-Buda, M.-C. Cyrille, O. Redon, and B. Dieny, Nature (London) **6**, 447 (2007).
[20] A. Dussaux *et al.*, Appl. Phys. Lett. **105**, 022404 (2014).
[21] J. E. Davies, O. Hellwig, E. E. Fullerton, G. Denbeaux, J. B. Kortright, and K. Liu, Phys. Rev. B **70**, 224434 (2004).
[22] J. H. Jung, B. Jeong, S. H. Lim, and S.-R. Lee, Appl. Phys. Express **3**, 023001 (2010).
[23] H. X. Yang, M. Chshiev, B. Dieny, J. H. Lee, A. Manchon, and K. H. Shin, Phys. Rev. B **84**, 054401 (2011).
[24] W. X. Wang, Y. Yang, H. Naganuma, Y. Ando, R. C. Yu, and X. F. Han, Appl. Phys. Lett. **99**, 012502 (2011).
[25] E. A. Jagla, Phys. Rev. B **72**, 094406 (2005).
[26] K. Janicka, J. D. Burton, and E. Y. Tsymbal, J. Appl. Phys. **101**, 113921 (2007).
[27] P. S. Fodor, G. M. Tsoi, and L. E. Wenger, J. Appl. Phys. **93**, 7438 (2003).
[28] A. Raghunathan, Y. Melikhov, J. Snyder, and D. Jiles, J. Magn. Magn. Mater. **324**, 20 (2012).
[29] J. C. L. Ribas, E. M. Lourenço, J. V. Leite, and N. J. Batistela, IEEE Trans. Magn. **49**, 1797 (2013).
[30] M. P. Seymour, I. Wilding, B. Xu, J. I. Mercer, M. L. Plumer, K. M. Poduska, A. Yethiraj, and J. van Lierop, Appl. Phys. Lett. **102**, 072403 (2013).
[31] A. P. S. Baghel and S. V. Kulkarni, J. Appl. Phys. **113**, 043908 (2016).
[32] A. Benassi and S. Zapperi, Phys. Rev. B **84**, 214441 (2011).
[33] M. Pardavi-Horvath, E. D. Torre, F. Vajda, and G. Vertesy, IEEE Trans. Magn. **29**, 3793 (1993).
[34] G. Bertotti, *Hysteresis in Magnetism for Physicist, Materials Scientists, and Engineers* (Academic Press, San Diego, 1998).
[35] A. Stancu, P. R. Bissell, and R. W. Chantrell, J. Appl. Phys. **87**, 8645 (2000).
[36] F. Liorzou, B. Phelps, and D. L. Atherton, IEEE Trans. Magn. **36**, 418 (2000).
[37] F. Vajda and E. D. Torre, IEEE Trans. Magn. **27**, 4757 (1991).
[38] A. Stancu, L. Stoleriu, and M. Cerchez, J. Appl. Phys. **89**, 7260 (2001).
[39] M. Cerchez, L. Stoleriu, and A. Stancu, Physica B **343**, 48 (2004).
[40] A. Stancu, C. Pike, L. Stoleriu, P. Postolache, and D. Cimpoesu, J. Appl. Phys. **93**, 6620 (2003).
[41] A. Muxworthy, D. Heslop, and W. Williams, Geophys. J. Int. **158**, 888 (2004).
[42] A. Muxworthy and W. Williams, J. Appl. Phys. **97**, 063905 (2005).
[43] A. Stancu, L. Stoleriu, P. Postolache, and M. Cerchez, IEEE Trans. Magn. **40**, 2113 (2004).
[44] G. Durin and S. Zapperi, *The Science of Hysteresis* (Academic Press, Amsterdam, 2006), Vol. 2.
[45] G. Bertotti, *Magnetic Hysteresis in Novel Magnetic Materials*, NATO Science Series E Vol. 338 (Kluwer Academic Publishers, Dordrecht, 1997), p. 125.
[46] A. Schwarz, M. Liebmann, U. Kaiser, R. Wiesendanger, T. W. Noh, and D. W. Kim, Phys. Rev. Lett. **92**, 077206 (2004).
[47] M. Liebmann, A. Schwarz, U. Kaiser, R. Wiesendanger, D.-W. Kim, and T.-W. Noh, Phys. Rev. B **71**, 104431 (2005).
[48] D. L. Atherton, B. Szpunar, and J. A. Szpunar, IEEE Trans. Magn. **23**, 1856 (1987).
[49] Z. Wlodarski, Physica B **373**, 323 (2006).
[50] H. Gong, D. Litvinov, T. J. Klemmer, D. N. Lambeth, and J. K. Howard, IEEE Trans. Magn. **36**, 2963 (2000).
[51] R. Law, R. Sbiaa, T. Liew, and T. C. Chong, Appl. Phys. Lett. **91**, 242504 (2007).
[52] R. Sbiaa and R. W. Chantrell, J. Appl. Phys. **117**, 17C102 (2015).
[53] O. Hellwig, T. L. Kirk, J. B. Kortright, A. Berger, and E. E. Fullerton, Nat. Mater. **2**, 112 (2003).
[54] D.-T. Ngo, D.-T. Quach, Q.-H. Tran, K. Mohave, T.-L. Phan, and D.-H. Kim, J. Phys. D: Appl. Phys. **47**, 445001 (2014).
[55] M. Labrune, S. Andrieu, F. Rio, and P. Bernstein, J. Magn. Magn. Mater. **80**, 211 (1989).
[56] M.-Y. Im, P. Fischer, T. Eimüller, G. Denbeaux, and S.-C. Shin, Appl. Phys. Lett. **83**, 4589 (2003).
[57] S. Konings, J. Miguel, J. Goedkoop, J. Camarero, and J. Vogel, J. Appl. Phys. **100**, 033904 (2006).
[58] R. Sbiaa, Z. Bilin, M. Ranjbar, H. K. Tan, S. J. Wong, S. N. Piramanayagam, and T. C. Chong, J. Appl. Phys. **107**, 103901 (2010).
[59] C. Kittel, Rev. Mod. Phys. **21**, 541 (1949).

[60] M. Pardavi-Horvath, G. Zheng, G. Vertesy, and A. Magni, IEEE Trans. Magn. **32**, 4469 (1996).
[61] P. Postolache, M. Cerchez, L. Stoleriu, and A. Stancu, IEEE Trans. Magn. **39**, 2531 (2003).
[62] A. Stancu, L. Stoleriu, P. Postolache, and R. Tanasa, J. Magn. Magn. Mater. **290-291**, 490 (2005).
[63] E. D. Torre, J. Oti, and G. Kadar, IEEE Trans. Magn. **26**, 3052 (1990).
[64] E. D. Torre and F. Vajda, IEEE Trans. Magn. **30**, 4987 (1994).
[65] E. Cardelli, A. Faba, G. Finocchio, and B. Azzerboni, IEEE Trans. Magn. **48**, 3367 (2012).
[66] I. Nová, V. Havlíček, and I. Zemánek, IEEE Trans. Magn. **49**, 148 (2013).
[67] C. Liu, E. R. Moog, and S. D. Bader, Phys. Rev. Lett. **60**, 2422 (1988).
[68] Z. Diao, E. R. Nowak, G. Feng, and J. M. D. Coey, Phys. Rev. Lett. **104**, 047202 (2010).
[69] K. De'Bell, A. B. MacIsaac, and J. P. Whitehead, Rev. Mod. Phys. **72**, 225 (2000).
[70] G. Szabo and G. Kadar, Phys. Rev. B **58**, 5584 (1998).
[71] A. F. Franco, J. L. Déjardin, and H. Kachkachi, J. Appl. Phys. **116**, 243905 (2014).
[72] D. A. Gilbert, G. T. Zimanyi, R. K. Dumas, M. Winklhofer, A. Gomez, N. Eibagi, J. L. Vicent, and K. Liu, Sci. Rep. **4**, 4204 (2014).
[73] C. Fowley, N. Decorde, K. Oguz, K. Rode, H. Kurt, and J. M. D. Coey, IEEE Trans. Magn. **46**, 2116 (2010).
[74] J. H. Jung, S. H. Lim, and S. R. Lee, Appl. Phys. Lett. **96**, 042503 (2010).
[75] S. Pal, B. Rana, O. Hellwig, T. Thomson, and A. Barman, Appl. Phys. Lett. **98**, 082501 (2011).
[76] J. H. Jung, S. H. Lim, and S.-R. Lee, J. Nanosci. Nanotechnol. **11**, 6233 (2011).